Ionic transport and heat capacity of glass-forming metal-nitrate mixtures

Andrei Pimenov, Peter Lunkenheimer, Michael Nicklas, R. Böhmer, Alois Loidl, C. A. Angell

Ionic transport and heat capacity of glass-forming metal–nitrate mixtures

A. Pimenov [a], P. Lunkenheimer [a,*], M. Nicklas [a], R. Böhmer [b], A. Loidl [a], C.A. Angell [c]

[a] *Universität Augsburg, Experimentalphysik V, D-86135 Augsburg, Germany*
[b] *Institut für Physikalische Chemie, Johannes Gutenberg-Universität, D-55099 Mainz, Germany*
[c] *Department of Chemistry, Arizona State University, Tempe, AZ 85287-1604, USA*

1. Introduction

Although the technology of vitrification is well known since archeological times and despite the fact that glass formation by viscous slow down is widely used for a large variety of technical applications, the microscopic mechanism that underlies the glass transition is still far from being understood. Consequently, studies on the glassy relaxation in complex materials are an area of active research, see for example Ref. [1]. Study of glass-forming ionic melts is highly attractive as these simple supercooled liquids can be approximated as hard sphere systems which are the subject of recent glass transition theories [2]. Melts of randomly close-packed ions are expected to belong to the class of fragile glassformers in the classification scheme introduced by Angell [3]. These materials show pronounced thermodynamic anomalies in the vicinity of the glass transition and sizable deviations from simple thermally activated behavior of the primary relaxational response. The ionic melt studied most thoroughly so

* Corresponding author. Tel.: +49-821 598 3603; fax: +49-821 598 3649; e-mail: peter.lunkenheimer@physik.uni-augsburg.de.

far is the mixed ionic glass-former $[Ca(NO_3)_2]_{0.4}[KNO_3]_{0.6}$ (CKN) (e.g., Refs. [4–13]). In addition to many investigations dealing with the systematics of the primary relaxational response near the glass transition, also the fast dynamics of CKN was studied extensively using neutron [6,7], light scattering [8,9], and dielectric spectroscopy [10–13]. There exists a large variety of other metal–nitrate mixtures which also can be easily vitrified [14] but which so far have found much less attention.

We report dielectric investigations of mixed nitrate glass-formers $[Ca(NO_3)_2]_{0.4}[RbNO_3]_{0.6}$ (CRN), $[Mg(NO_3)_2]_{0.44}[KNO_3]_{0.56}$ (MKN), $[Mg(NO_3)_2]_{0.44}[NaNO_3]_{0.56}$ (MNN) at frequencies up to 300 MHz and compare them to the results previously obtained for CKN. The present work deals mainly with the relaxational response of these melts and glasses as obtained via dielectric spectroscopy; the results at high frequencies ($\nu > 100$ MHz) will be given in a forthcoming paper. In addition, we report preliminary results of specific heat measurements at low temperatures.

2. Experimental details

The schematic phase diagrams of the mixed nitrates under investigation are shown in Fig. 1 [14].
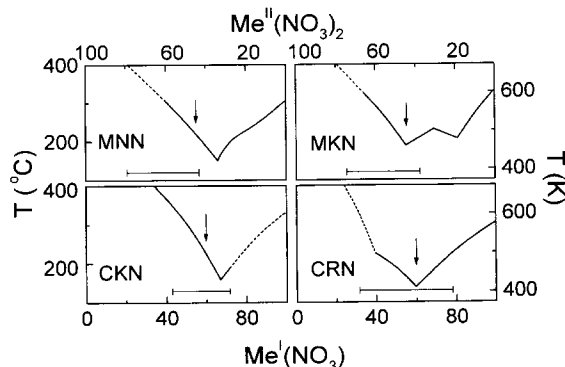

Fig. 1. Schematic phase diagrams of $[Mg(NO_3)_2]_x[NaNO_3]_{1-x}$, $[Ca(NO_3)_2]_x[KNO_3]_{1-x}$, $[Mg(NO_3)_2]_x[KNO_3]_{1-x}$, and $[Ca(NO_3)_2]_x[RbNO_3]_{1-x}$ (adapted from Ref. [14]). The lower and the upper scale gives the concentration (in mol%) of the mono- and divalent metal ion, respectively. The horizontal bars indicate the composition range in which glasses can be obtained. The arrows show the concentrations investigated in the present work.
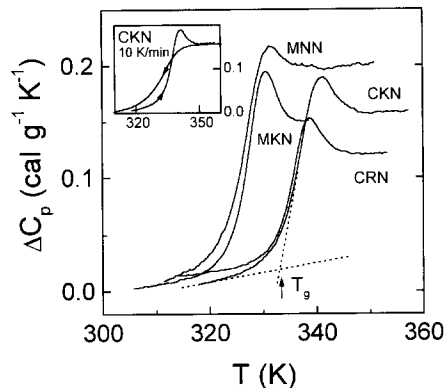

Fig. 2. Results of DSC scans obtained at a heating rate of 10 K/min after a prior cooling with the same rate. The inset shows the result of a complete scan (including cooling) for CKN. The resulting glass temperatures, T_g, which have been determined as indicated in the figure are listed in Table 1.

The horizontal bars indicate composition ranges in which glasses can be obtained [14]. The arrows indicate the concentrations which have been studied in the present work.

$Ca(NO_3)_2 \cdot 4H_2O$ (> 99%), $Mg(NO_3)_2 \cdot 6H_2O$ (> 99%), $Na(NO_3)$ (> 99%), $K(NO_3)$ (> 99%) from Merck, and $Rb(NO_3)$ (> 99%) from Fluka were fused and dehydrated at 510 K usually for at least one day in a vacuum furnace. The samples were then transferred immediately into an argon box and handled under argon or vacuum. The samples were characterized using differential scanning calorimetry with a heating rate of 10 K/min after a prior cooling with the same rate. Results of heating scans are given in Fig. 2. The inset shows both the cooling and the heating curve obtained for CKN. The calorimetric glass temperatures T_g which were obtained from the heating curves (cf. Fig. 2) are given in Table 1. In the calorimetric measurements the glass-transition temperature was determined with an uncertainty of ±2 K. The accuracy of the experiments did not allow measurement of rate dependence of the glass transition temperature with sufficient accuracy, in order to determine the activation enthalpy.

Most experiments in the liquid state were performed using a constant cooling rate of about 0.5 K/min. The ion conducting nitrates investigated in this work exhibit an enhanced tendency to crystallize in certain temperature ranges above T_g. Near these

temperatures the measurements were carried out for cooling and heating rates of about 2 K/min. Nevertheless, occasionally crystallization occurred even at those rates. For the variation of temperature a nitrogen gas-heating system ($100 \text{ K} \leq T \leq 600 \text{ K}$) and home-built ovens have been used.

Low-frequency measurements at $10^{-2} \text{ Hz} \leq \nu \leq 1$ kHz were carried out using a Schlumberger 1260 impedance analyzer in conjunction with a Chelsea dielectric interface. At $20 \text{ Hz} \leq \nu \leq 1$ MHz, a HP4284 autobalance bridge was used. In both cases the sample material was placed between stainless steel plates, 20 mm in diameter and with a distance of approximately 1 mm, which were highly polished to impede crystallization. For frequencies $\nu \geq 1$ MHz a reflection technique was used employing a HP4191 network analyzer. Here the sample was placed at the end of the inner conductor of a coaxial line and was shorted with the outer conductor by a stainless steel plate. From the complex reflection coefficient of this assembly the complex dielectric constant and the conductivity of the sample can be calculated after proper calibration to determine residual reflections and phase shifts. The specific heat experiments were performed in an adiabatic Nernst calorimeter at temperatures $3 \text{ K} \leq T \leq 40$ K. The samples had a typical mass of 1 g and were covered by a thin film of Apiezon 'N' grease to prevent ambient air contact.

3. Results

Fig. 3 shows the frequency dependence of the real part of the conductivity σ' (upper frame) and of the dielectric constant ϵ' (lower frame) as measured in CRN for various temperatures. The conductivity exhibits the typical signatures of an ionic conductor: a frequency-independent dc plateau is followed by a power-law increase of the ac conductivity at higher frequencies. The transition from dc to ac behavior shifts to higher frequencies for higher temperatures. For frequencies to approximately 2.5 decades above the transition region, $\sigma'(\nu)$ can well be described by the expression, $\sigma' = \sigma_{dc} + \sigma_0 \nu^s$ as demonstrated by the solid lines in Fig. 3. Such a behavior, termed 'universal dielectric response' (UDR) [15,16], has been found in a vast variety of disordered materials among which are many ionic conductors. With s

Table 1
Parameters characterizing the ionic motion in $[Ca(NO_3)_2]_{0.4}[KNO_3]_{0.6}$ (CKN) [5,12,13], $[Ca(NO_3)_2]_{0.4}[RbNO_3]_{0.6}$ (CRN), $[Mg(NO_3)_2]_{0.44}[KNO_3]_{0.56}$ (MKN), and $[Mg(NO_3)_2]_{0.44}[NaNO_3]_{0.56}$ (MNN). T_g is the calorimetric glass temperature as obtained from DSC experiments, performed with a heating rate of 10 K/min (Fig. 2). ϵ_x denotes the high-frequency dielectric constant. E, T_{VF}, τ_0, and ρ_0 are the hindering barrier, Vogel–Fulcher temperature, attempt frequency and resistance prefactor, respectively, as obtained from simultaneous fits of $\tau_\sigma(T)$ and $\rho_{dc}(T)$ in the liquid state (cf. Fig. 4) using the Vogel–Fulcher law. E_g denotes the hindering barrier in the glass state and D the strength index [27]. $R = 100s/\tau_\sigma(T_g)$ is the decoupling index (see text). β is the stretching parameter below T_g. The values in brackets for E, T_{VF}, and D denote the results of fits where τ_0 has been kept constant ($\tau_0 = 3.2 \times 10^{-14}$ s) for all systems (dashed lines in Fig. 4). The variation from the results of the free fits indicate how the fits are influenced by the transition region at T_g and gives an estimate of the error bars

	CKN	CRN	MKN	MNN
T_g (K)	333 (± 2)	333 (± 2)	324 (± 2)	323 (± 2)
E/k_B (K)	1500 (1210)	1020 (1190)	1060 (1170)	1730 (1240)
T_{VF} (T)	283 (291)	294 (289)	295 (292)	264 (282)
D	5.3 (4.1)	3.5 (4.1)	3.6 (4.0)	6.6 (4.4)
τ_0 (s)	$5.3(\pm 1) \times 10^{-15}$	$5.1(\pm 1) \times 10^{-14}$	$6.9(\pm 1.5) \times 10^{-14}$	$2.4(\pm 0.5) \times 10^{-15}$
ρ_0 (Ω cm)	$6.4(\pm 1.5) \times 10^{-3}$	$7.0(\pm 1.5) \times 10^{-2}$	$10(\pm 2) \times 10^{-2}$	$3.9(\pm 0.5) \times 10^{-3}$
ϵ_x	8.2 (± 0.2)	7.8 (± 0.2)	6.7 (± 0.2)	6.5 (± 0.2)
$\tau_0/(\rho_0 \epsilon_0)$	9 (± 2)	8 (± 2)	8 (± 2)	7 (± 2)
E_g/k_B (K)	13 000 (± 1000)	12 900 (± 500)	22 000 (± 2000)	11 400 (± 500)
$\log_{10} R$	3.9 (± 0.3)	4.1 (± 0.3)	2.0 (± 0.3)	3.7 (± 0.3)
β (glass)	0.7 (± 0.03)	0.76 (± 0.03)	0.71 (± 0.03)	0.77 (± 0.03)

being about 0.7, the frequency exponent of CRN lies in the range of values found for other ionic conductors. Usually such a power law behavior of $\sigma'(\nu)$ is ascribed to hopping processes for which various models have been proposed, see for example Ref. [17,18].

At frequencies well above the transition regime, $\sigma'(\nu)$ shows clear deviations from UDR behavior exhibiting a slope s which increases with frequency and reaches values near unity. This implies a frequency independent dielectric loss which should be seen most clearly at low temperatures in experiments providing a sufficiently broad frequency range. By combining the conductivity results from various techniques, such a constant loss behavior has very early been assumed to be a universal feature of glasses by Wong and Angell [19]. Recently it has been shown to exist also in crystalline ionic conductors and has been termed 'second universality' [20]. For the highest frequencies investigated, a slope s even larger than unity shows up which in consequence leads to a slight minimum of the dielectric loss (not shown). This feature, which similarly shows up for CKN, has been discussed in detail elsewhere [12,13].
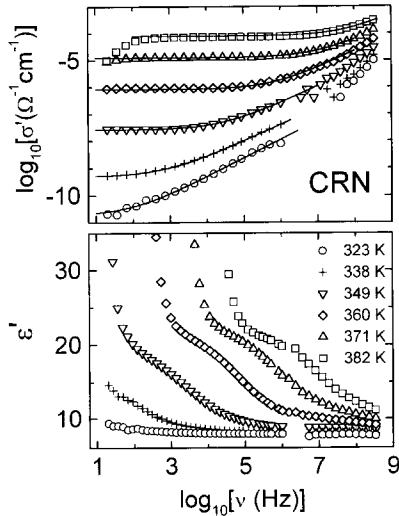

Fig. 4. Temperature dependence of the dc resistivity, ρ_{dc}, (open symbols) and the average conductivity relaxation time, $\langle \tau_\sigma \rangle$, (closed symbols) for CKN, CRN, MKN, and MNN in an Arrhenius representation. The dc resistivity has been obtained from the inverse saturation value of $\sigma'(\nu)$ (Fig. 3). The experimental error bars are smaller than the symbols used. The solid lines are the results of least square fits using the Vogel–Fulcher law which have been performed simultaneously on $\rho_{dc}(T)$ and $\tau_\sigma(T)$. The fit parameters are given in Table 1. The dashed lines are fits with τ_0 fixed at 3.2×10^{-14} s for all systems (parameters in brackets in Table 1).

Fig. 3. Frequency dependence of the real part of the conductivity, σ', and dielectric constant, ϵ', of CRN for various temperatures. The experimental error bars are smaller than the symbols used. The lines in the upper frame are the results of fits using the UDR.
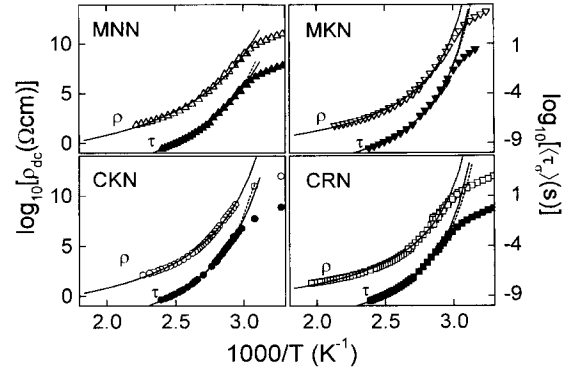
An additional feature of $\sigma'(\nu)$, seen for the two highest temperatures plotted in Fig. 3, is a decrease of σ' for frequencies below the saturation range shifting out of the frequency window for the lower temperatures. This is also a typical finding for ionic conductors and can be ascribed to space charges at blocking electrodes, an effect which becomes increasingly important at high temperatures, i.e., in the regime of high mobilities of the charge carriers [21].

The conductivities as measured in MKN and MNN behave qualitatively similar to that of CRN. In Fig. 4 the dc resistivity, $\rho_{dc} = 1/\sigma_{dc}$, as determined from the dc plateau of $\sigma'(\nu)$ is plotted in an Arrhenius representation for the three nitrates under investigation and compared to CKN [5,12]. In all cases ρ_{dc} clearly deviates from thermally activated behavior with very similar absolute values of ρ_{dc} in the liquid state. At high temperatures, $T > T_g$, σ_{dc} can be described by a Vogel–Fulcher (VF) law (solid lines in Fig. 4, however, for limitations, see Ref. [22]). Below T_g, $\sigma_{dc}(T)$ levels off to an Arrhenius type of behavior with a much lower effective energy barrier. This is the temperature regime where the environ-

ment of the mobile ions becomes static on the time scale set by the experiment [5] as will be discussed below in more detail.

The dielectric constant ϵ' of CRN (lower frame of Fig. 3) rises with decreasing frequency with a tendency to level off at intermediate frequencies. In the liquid phase and at low frequencies a dramatic increase by several orders of magnitude sets in (not shown in Fig. 3). For lower temperatures this increase becomes successively smaller and for the lowest temperatures shown in Fig. 3, $\epsilon'(\nu)$ becomes almost constant approaching its high frequency limit ϵ_x which is listed in Table 1. The huge increase of $\epsilon'(\nu)$ is a typical consequence of the formation of space charges near the electrodes which also affects the conductivity as mentioned above. It is well known that the blocking electrode effects show up in $\epsilon'(\nu)$ at much higher frequencies than in $\sigma'(\nu)$ as indeed observed here [21]. The leveling off of $\epsilon'(\nu)$ at intermediate frequencies is a characteristic feature of relaxational processes. Similar dependences of ϵ' have been reported for CKN [5,12,23]. However, for MKN and MNN such phenomena could not be ob-

Fig. 6. Same as Fig. 5 for MKN.

served which was due to more pronounced blocking electrode effects in these materials. These can be ascribed to the occasional occurrence of small air gaps arising between sample and electrodes at low temperatures. They are due to thermal contraction and lead to a strong increase of ϵ' at low frequencies similar to electrode blocking. However these phenomena do not affect the results at higher frequencies.

The relaxation feature found for CRN in $\epsilon'(\nu)$ does not show up in the frequency dependence of the dielectric loss, ϵ'', but is obscured by the contributions of the dc conductivity. It is an interesting feature of the spectra in Fig. 3 that for all temperatures the point of inflection of $\epsilon'(\nu)$ which is a measure for the associated relaxation time is located at frequencies that correspond to the transition region from dc to ac behavior in $\sigma'(\nu)$. This indicates a close connection of mechanisms responsible for dc and ac conductivity.

A commonly employed method to obtain information about the dynamics of the charge carriers in ionic conductors is the use of modulus formalism [23] where the complex electrical modulus $M^* := 1/\epsilon^*$ is analyzed. In using the modulus representation, the effects of blocking electrodes are usually fully suppressed. However, it has to be mentioned
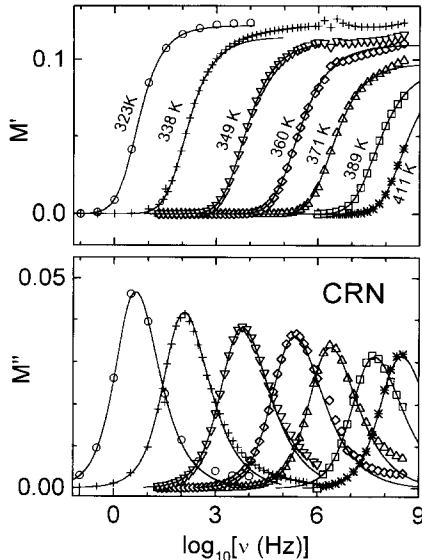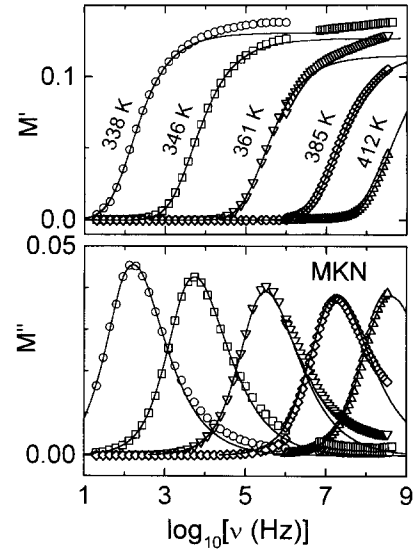

Fig. 5. Frequency dependence of real and imaginary part of the electric modulus M of CRN for various temperatures. The experimental error bars are smaller than the symbols used. The solid lines are the results of least square fits using the Fourier transform of the KWW function which have been performed simultaneously on $M'(\nu)$ and $M''(\nu)$.

Fig. 7. Same as Fig. 5 for MNN.

Fig. 8. Temperature dependence of the specific heat at constant pressure, C_p, for CKN, MKN, and MNN in a double logarithmic representation of C_p/T^3 vs. T. The experimental error bars are smaller than the symbols used. The inset shows the data for CKN obtained in the present work together with data measured at lower temperatures from Ref. [41]. For comparison the specific heat of vitreous SiO_2 (from Ref. [40]) is shown as solid line.
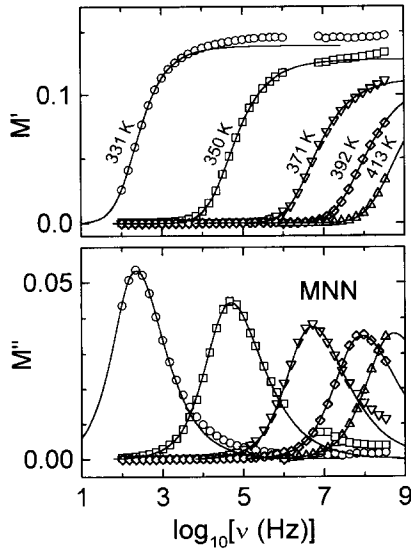
that there is an ongoing controversy concerning the applicability of this formalism, see for example Ref. [24–26]. Figs. 5–7 show the real and imaginary parts of M^* for CRN, MKN, and MNN, respectively. As is typical for ionic conductors, the real part, M', exhibits a steplike increase with increasing frequency which is accompanied by well defined peaks in the imaginary part, M'', located at the point of inflection of $M'(\nu)$. Both features shift to higher frequencies with increasing temperature. By the relation $2\pi\nu_p\tau_\sigma \approx 1$, the frequency of the peak maximum ν_p in $M''(\nu)$ gives a measure for the so-called conductivity relaxation time, τ_σ, which is assumed to represent a characteristic time scale of the ionic motion [21]. The frequency dependence of the electric modulus is usually analyzed using the Fourier transform of the KWW function $\Phi(t) = \Phi_0 \exp[-(t/\tau_\sigma)^\beta]$. The lines in Figs. 5–7 are the results of fits performed simultaneously on M' and M'' using this function. A reasonably good agreement of data and fit has been obtained for frequencies below and approximately one decade above the peak maximum of $M''(\nu)$. At higher frequencies deviations show up which for both, real and imaginary part, lead to an underestimation of the measured values. This is a common finding for ionic conductors. At frequencies above 100 MHz and temperatures below about 360 K,
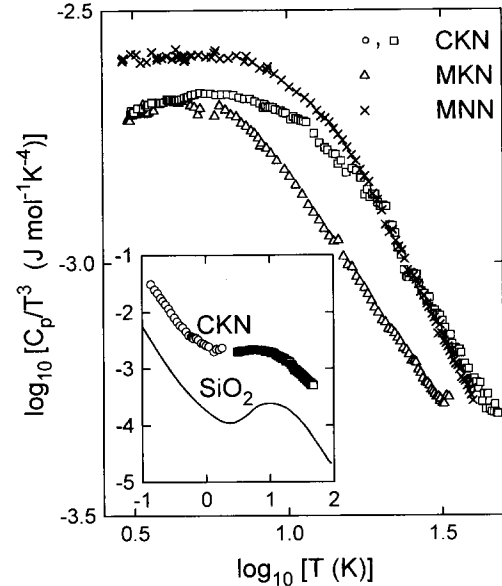
indications of a minimum in $M''(\nu)$ (and consequently also in $\epsilon''(\nu)$ which is proportional to M'' at frequencies $\nu \gg \nu_p$) show up (Fig. 5). A similar
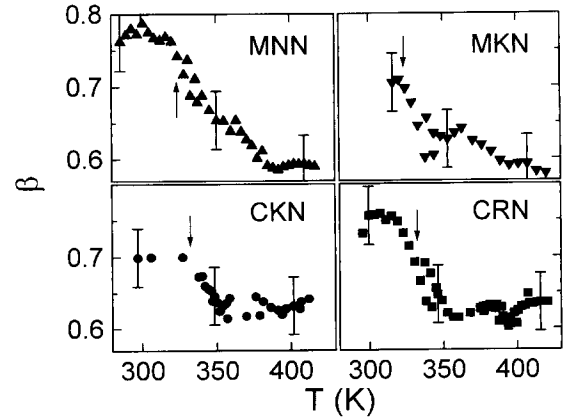

Fig. 9. Temperature dependence of the stretching parameter β for all four nitrate mixtures as obtained from the fits of $M(\nu)$. The results for CKN are taken from Ref. [12]. The arrows indicate the glass temperatures.

minimum in $M''(\nu)$ and $\epsilon''(\nu)$ has recently been reported for CKN and compared to various theoretical concepts [12]. A detailed investigation of high-frequency dielectric properties of CKN and CRN has been published elsewhere [13].

Temperature dependences of heat capacity C_p for CKN, MKN, and MNN were investigated in a quasiadiabatic calorimeter for temperatures $3\ K \le T \le 40\ K$. The results are plotted in Fig. 8 as C_p/T^3 vs. T in a double-logarithmic representation. For all samples, C_p/T^3 steadily increases with decreasing temperatures and reaches a plateau for $T < 10\ K$.

4. Discussion

From fitting parameters τ_σ and β, the average conductivity relaxation time $\langle \tau_\sigma \rangle$ can be calculated using $\langle \tau_\sigma \rangle = \tau_\sigma / \beta \Gamma(1/\beta)$ where Γ denotes the gamma function. In Fig. 4 the temperature dependence of $\langle \tau_\sigma \rangle$ is plotted in an Arrhenius representation for CKN [5,12], CRN, MKN, and MNN. The temperature dependence resembles that of the dc resistivity which is also shown in Fig. 4 (note that the scaling of the logarithmic axes of ρ_{dc} and τ_σ is the same). Clearly, all nitrate mixtures exhibit pronounced deviations of $\langle \tau_\sigma(T) \rangle$ from thermally activated behavior as is typical for fragile glass-formers [3,27]. The solid lines in Fig. 4 are the results of fits using the VF law, $\tau = \tau_0 \exp(E/k_B(T - T_{VF}))$, and $\rho = \rho_0 \exp(E/k_B(T - T_{VF}))$, which have been performed simultaneously for $\langle \tau_\sigma(T) \rangle$ and $\rho_{dc}(T)$. For all four nitrate mixtures, in the liquid state both quantities can be well described with VF parameters given in Table 1. The difference of parameters obtained for the four nitrates should not be overemphasized as they depend on the temperature region (points near T_g where the VF law fails) used for the fit. A reasonable description of the data in Fig. 4 is also possible with almost identical VF parameters for all four materials. The dashed lines in Fig. 4 represent fits of τ_σ using a constant $\tau_0 = 3.2 \times 10^{-14}$ s for all systems resulting in similar VF parameters (values in brackets in Table 1). In the modulus formalism [23] the ratio of $\langle \tau_\sigma \rangle$ and ρ_{dc} is connected to the high-frequency limit of the dielectric constant by $\langle \tau_\sigma \rangle / \rho_{dc} = \epsilon_0 \epsilon_\infty$ (ϵ_0 the permittivity of free space). The observed proportionality of $\langle \tau_\sigma \rangle$ and ρ_{dc} (Fig.

4) is consistent with the only weakly temperature dependent high-frequency permittivity ϵ_∞. In Table 1 we list $\tau_0/(\rho_0 \epsilon_0)$ which agrees rather well with the experimentally obtained value of ϵ_∞.

At temperatures close to the calorimetric glass temperatures, $\tau_\sigma(T)$ and $\rho_{dc}(T)$ exhibit abrupt changes of slope. The temperature of this anomaly can be identified with the glass temperature T_g' for the timescale set by the experiment [5]. This break in slope can be rationalized by the notion that above T_g' two hindering barriers add up to the observed activation energy: the hindering barrier against the rearrangement of the surrounding liquid structure and that for the motion of the ionic charge carriers through channels provided by the environment. Below T_g' the environment of the charge carriers is frozen on the timescale of the experiment leading to a significantly smaller activation energy [5] (see Table 1).

To give a quantitative measure of the fragility of glass-formers, a strength parameter $D_\sigma = E/T_{VF}$ can be calculated from the VF parameters describing the conductivity relaxation [3,27]. Values of D_σ (Table 1) characterize the molten nitrates as fragile glass-formers. However, one has to be aware that, due to decoupling of primary, structural relaxation (measured, for example, by the viscosity and characterized by a relaxation time τ_p) from the conductivity relaxation, the 'true' value of D may deviate from D_σ. Decoupling which is well established for CKN [5,12] can be expected to be most prominent below T_g where the charge carrying ions may be still mobile in channels provided by the lattice which is static on the experimental timescale.

A related approach to characterize the fragility of glass-formers is by the fragility parameter $m = d(\log_{10} \tau)/d(T_g/T)$ which is the slope of $\tau(T)$ at T_g in a scaled Arrhenius representation [28]. For CKN, from dynamical light scattering [29] and dynamic specific heat measurements [30] $m \approx 93$ has been determined [27] which is larger than $m_\sigma \approx 54$ as obtained from the slope of $\tau_\sigma(T)$ at T_g. If one accepts that τ_σ is a measure for the dynamics of the ions, another indication for the decoupling of primary and conductivity relaxation in the nitrate mixtures can be inferred from the finding that near the glass temperature, τ_σ is not equal to ~ 100 s as it should be for fully coupled responses. The decou-

pling indices $R := 100s/\tau_\sigma(T_g)$ are given in Table 1. R values between about 10^2 and 10^4 are obtained. It is noted that CKN, CRN, and MNN fit very well into the correlation scheme obtained by Angell [31] which connects the width parameter β in the glassy state (cf. Table 1) and the decoupling index R of ionic glasses. For MKN only a rough agreement is obtained.

In Fig. 9 the stretching exponents β as determined from the fits of $M''(\nu)$ are shown for CKN [5,12], CRN, MKN, and MNN. β determines the width and asymmetry of the modulus peaks. A value of $\beta = 1$ corresponds to single-exponential relaxation behavior. As seen in Fig. 9, in the liquid phase the stretching exponents of all nitrate mixtures investigated are temperature dependent with a clear tendency to decrease with increasing temperature as it has been found in some other glass formers, too [32]. $\beta(T)$ becomes approximately constant yielding a value of 0.6–0.7 which, for CKN, agrees well to the findings from other experimental techniques [6–9]. Even far in the liquid phase, $\beta(T)$ does not approach unity as could naively be expected having in mind the dynamical averaging usually associated with the very fast fluctuating environments in the ionic melt. This behavior seems to indicate that even in the liquid state the conductivity relaxation is not a single ion phenomenon but still is dominated by cooperative effects. However, in an ultrasonic study by Angell and Torell [33] it has been shown that for higher temperatures, $T \geq 500$ K, β indeed approaches unity.

A consequence of the modulus formalism is the prediction of the existence of a dielectric relaxation feature in $\epsilon'(T)$ (the corresponding anomaly in $\epsilon''(T)$ is hidden by the strong conductivity contributions). This follows from simple considerations of a non-exponential conductivity relaxation or if there is a distribution of relaxation times [23]. It has been shown [34] that in case the KWW function is assumed to describe the conductivity relaxation, the ratio of ϵ_∞ and the limiting low-frequency dielectric constant, ϵ_s, is given by: $\epsilon_s/\epsilon_\infty = \beta \, \Gamma(2/\beta)/\Gamma^2(1/\beta)$. For CKN and CRN with $\beta \approx 0.63$ in the relevant temperature range (Fig. 9), this ratio should be 1.9. This prediction is in reasonable agreement with the relaxation steps observed in CKN [5,12,35] and CRN (Fig. 3).

Finally, we will discuss the specific heat results of Fig. 8. In crystalline solids the specific heat follows a T^3 dependence at low temperatures which can be described in terms of the Debye heat capacity due to long-wavelength acoustic phonons. Amorphous materials are characterized by additional low-temperature contributions [36]: $C_p = c_1 T^\alpha + c_D T^3 + c_{exc}$. The first term is time dependent and almost linear in temperature ($\alpha \approx 1$). It can be ascribed to two-level tunneling excitations [37,38]. $c_D T^3$ is the Debye specific heat and c_{exc} is an excess contribution. In most glasses, c_{exc} shows up between 4 K and 20 K and is believed to result from an excess density of states due to localized vibrational excitations. In light- and neutron-scattering experiments this excess density of states shows up in the dynamical susceptibility and has been termed Boson peak. It has been pointed out by Sokolov et al. [39] that this excess peak is well developed for strong glass-formers, while a peak can hardly be detected in fragile systems. They defined Q, the ratio of C_p at the peak minimum and at the maximum which shows up between the excess contribution and the tunneling term. This ratio was found to be $Q \leq 0.5$ for strong and $Q \approx 1$ for fragile systems [39].

As a representative example we plotted C_p/T^3 vs. T for vitreous silica [40] (inset of Fig. 8) and compare these results with the heat capacity obtained for CKN. Here the low temperature values ($T < 2$ K, open circles) have been taken from a study by Raychaudhuri and Pohl [41]. The excess peak and the minimum are well developed in amorphous SiO_2 which is a strong glass-former. For CKN essentially only a plateau can be detected, characteristic for fragile liquids with $Q \approx 1$. Fig. 8 reveals that CKN, MKN and MNN exhibit a similar low-temperature heat capacity. Obviously, they all belong to the class of fragile systems which corresponds to the low strength index listed in Table 1.

5. Conclusions

The electrical properties of glass-forming metal–nitrate mixtures CRN, MKN, and MNN investigated are qualitatively and quantitatively similar to that of the thoroughly studied nitrate glass CKN. The behavior of the complex conductivity is typical for ionic

conductors and can well be described using predictions of the modulus formalism. At temperatures near T_g the primary response and the conductivity relaxation decouple. The temperature dependencies of the conductivity relaxation times and the excess peak in the specific heat are characteristic of fragile glass-formers.

Acknowledgements

References

[1] K.L. Ngai, E. Riande, G.B. Wright, eds., Relaxations in Complex Systems 2, J. Non-Cryst. Solids 172–174 (1994).

[2] W. Götze, L. Sjögren, Rep. Progr. Phys. 55 (1992) 241, and references therein.

[3] C.A. Angell, J. Chem. Phys. Solids 49 (1988) 863.

[4] C.A. Angell, J. Phys. Chem. 68 (1965) 218.

[5] F.S. Howell, R.A. Bose, P.B. Macedo, C.T. Moynihan, J. Phys. Chem. 78 (1974) 639.

[6] F. Mezei, W. Knaak, B. Farago, Phys. Rev. Lett. 58 (1987) 571.

[7] J. Wuttke, W. Petry, Trans. Theory Stat. Phys. 24 (1995) 1075.

[8] G. Li, W.M. Du, X.K. Chen, H.Z. Cummins, N.Z. Tao, Phys. Rev. A45 (1992) 3867.

[9] Y. Yang, K.A. Nelson, J. Chem. Phys. 104 (1996) 5429.

[10] K. Funke, J. Hermeling, J. Kümpers, Z. Naturforsch. 43a (1988) 1094.

[11] K.L. Ngai, C. Cramer, T. Saatkamp, K. Funke, Proc. Workshop on Non-Equilibrium Phenomena in Supercooled Fluids, Glasses, and Amorphous Materials, Pisa, Italy, 1995 (World Scientific, Singapore, 1996).

[12] A. Pimenov, P. Lunkenheimer, H. Rall, R. Kohlhaas, A. Loidl, R. Böhmer, Phys. Rev. E54 (1996) 676.

[13] P. Lunkenheimer, A. Pimenov, A. Loidl, Phys. Rev. Lett. 78 (1997) 2995.

[14] E. Thilo, C. Wieker, W. Wieker, Silikattechn. 15 (1964) 109.

[15] A.K. Jonscher, Nature 267 (1977) 673.

[16] A.K. Jonscher, Dielectric Relaxation in Solids (Chelsea Dielectric, London, 1983).

[17] S.R. Elliott, A.P. Owens, Philos. Mag. B60 (1989) 777.

[18] K. Funke, Philos. Mag. A64 (1991) 1025.

[19] J. Wong, C.A. Angell, Glass: Structure by Spectroscopy (Marcel Dekker, New York, 1974) p. 723.

[20] W.K. Lee, J.F. Liu, A.S. Nowick, Phys. Rev. Lett. 67 (1991) 1559.

[21] J.R. MacDonald, ed., Impedance Spectroscopy – Emphasizing Solid Materials and Systems (Wiley, New York, 1987).

[22] R. Bose, R. Weiler, P.B. Macedo, Phys. Chem. Glasses 11 (1970) 117.

[23] P.B. Macedo, C.T. Moynihan, R. Bose, Phys. Chem. Glasses 13 (1972) 171.

[24] C.T. Moynihan, J. Non-Cryst. Solids 172–174 (1994) 1395.

[25] S.R. Elliott, J. Non-Cryst. Solids 170 (1994) 97.

[26] D.L. Sidebottom, P.F. Green, R.K. Brow, J. Non-Cryst. Solids 183 (1995) 151.

[27] C.A. Angell, in: Relaxation in Complex Systems, ed. K.L. Ngai and G.B. Wright (Office of Naval Research, Washington, DC, 1984) p. 3.

[28] R. Böhmer, K.L. Ngai, C.A. Angell, D.J. Plazek, J. Chem. Phys. 99 (1993) 4201.

[29] E.A. Pavlatou, A.K. Rizos, G.N. Papatheodorou, G. Fytas, J. Chem. Phys. 94 (1991) 224.

[30] R. Böhmer, E. Sanchez, C.A. Angell, J. Phys. Chem. 96 (1992) 9089.

[31] C.A. Angell, Chem. Rev. 90 (1990) 523.

[32] W.C. Hasz, C.T. Moynihan, P.A. Tick, J. Non-Cryst. Solids 172–174 (1994) 1363.

[33] C.A. Angell, L.M. Torell, J. Chem. Phys. 78 (1983) 937.

[34] C.T. Moynihan, L.P. Boesch, N.L. Laberge, Phys. Chem. Glasses 14 (1973) 122.

[35] R. Kohlhaas, unpublished.

[36] R.C. Zeller, R.O. Pohl, Phys. Rev. B4 (1971) 2029.

[37] W.A. Phillips, J. Low Temp. Phys. 7 (1972) 351.

[38] P.W. Anderson, B.I. Halperin, C.M. Varma, Philos. Mag. 25 (1972) 1.

[39] A.P. Sokolov, A. Kisliuk, D. Quitmann, A. Kudlik, E. Rössler, J. Non-Cryst. Solids 172–174 (1994) 138.

[40] W.A. Phillips, Rep. Prog. Phys. 50 (1987) 1657.

[41] A.K. Raychaudhuri, R.O. Pohl, Phys. Rev. B25 (1982) 1310.